Real-Time Detection of an Aircraft Deep Stall and Recovery Procedure

Sébastien Kolb, Olivier Montagnier, Laurent Hetru, Thierry Faure

Real-time detection of an aircraft deep stall and recovery procedure

Sébastien Kolb*, Olivier Montagnier†, Laurent Hétru‡ and Thierry M. Faure§
Air Force Research Center (CReA), French Air Force Academy, Salon-de-Provence, France

I. Nomenclature

c	=	main wing chord	m
C_L	=	lift aerodynamic coefficient	-
C_D	=	drag aerodynamic coefficient	-
C_m	=	pitching moment aerodynamic coefficient	-
I_y	=	moment of inertia about the y-axis	kg m^2
m	=	mass	kg
q	=	pitch rate	rad/s
S	=	reference main wing area	m^2
T	=	thrust	N
$\mathbf{U}$	=	input vector	-
V	=	airspeed	m/s
$\mathbf{X}$	=	state vector	-
α	=	angle-of-attack	°
γ	=	flight-path-angle	°
δ_e	=	elevator deflection angle	°
δ_f	=	flap deflection angle	°
δ_T	=	thrust throttle	-
δ_{sm}	=	static margin	%
λ	=	eigenvalue	-
ρ	=	air density	kg/m^3
ζ	=	damping	-

II. Introduction

Deep stall is a kind of stall affecting aircraft longitudinal dynamics. It corresponds to a stable equilibrium at high angle-of-attack (AoA) for which the pitch control surface is almost or totally ineffective [1, 2]. Deep stall is a hazardous aircraft loss-of-control which implies an established stall flight with high descent velocities and no easy recovery procedure. In the history of aeronautics, several aircraft have encountered this type of stall leading to crashes, more especially during flight tests (e.g. Javelin Gloster, BAC 1-11, Canadair Regional Jet 600 [3], etc.).

The existence of this equilibrium depends on aircraft design factors and on some peculiar flight conditions. Taylor and Ray [4, 5] have studied several aircraft designs in a wind tunnel to identify geometrical factors promoting deep stall risk. They noticed that T-tail or aft mounted engines are critical factors. The flight of the T-tail inside the separated wake of the stalled main wing is generally considered as an explanation of the phenomenon [4–7]. Byrnes *et al.* [8] have studied the impact of T-tail position and surface, and swept wing angle on the aircraft aerodynamics and flight

*Assistant Professor, Centre de Recherche de l'Armée de l'Air, French Air Force Academy/sebastien.kolb@ecole-air.fr
†Assistant Professor, Centre de Recherche de l'Armée de l'Air, French Air Force Academy/olivier.montagnier@ecole-air.fr
‡Research Assistant, Centre de Recherche de l'Armée de l'Air, French Air Force Academy/laurent.het@free.fr
§Associate Professor, Centre de Recherche de l'Armée de l'Air, French Air Force Academy/thierry.faure@ecole-air.fr

dynamics. In these experiments, deep stall equilibrium occurs for T-tail and classical small tail configurations but only in the case of swept main wings. Swept wings induce pitch-up effect after stall leading to deep stall equilibrium [9, 10].

Nevertheless, in the last decade, several aircraft (e.g. Airbus A400M, Comac ARJ21, Beechcraft 1900, Bombardier CRJ1000, etc.) and also small unmanned aerial vehicle (UAV) have been designed with a T-tail and sometimes with aft mounted engines. In general, the normal laws of aircraft are protected from high AoA (AoA protection) as in the case of the C-17A [11]. Other airplanes have a stick pusher or a stick shaker to prevent such dangerous situations. In spite of everything, some flights involve high AoA like flight tests for a new aircraft which necessarily reach the stall or post stall regions. For an aircraft potentially presenting a deep stall risk, a "deep stall recovery system" (rocket, parachute, etc.) is generally implemented to get out from deep stall equilibrium if necessary [12]. But this kind of device can be fatal if it is activated at the wrong time instant. Another case concerns peculiar system failures involving alternate law (or secondary law) where AoA protection is switched off as in the flight crash AF447 Rio-Paris. The final report on the accident [13] states that the AoA had reached 40°. Lastly, in normal flight conditions, some inertial and aerodynamic aircraft configurations, possibly combined, can also lead to deep stall entry such as bad aft center balance, overload, unexpected high-lift devices use.

Therefore, in accordance with Goman [14], it is interesting to know as soon as possible the precursory signs of deep stall entry in order to implement a warning for this kind of untypical situation follow-up and an automatic or manual procedure to escape from this hazardous phenomenon. Recently, several works have concerned the analysis of deep stall dynamics applying bifurcation theory [15–20], others have concerned the analysis of deep stall landing for UAV [21–23] but none concern the real-time detection of deep stall and recovery procedure. On the other hand, due to the development of more and more autonomous aircraft, many recent works concern the loss-of-control prevention, detection and recovery [24–26]. Deep stall studies are generally carried out with the assumption of longitudinal flight and such hypothesis is adopted hereafter. However, an asymmetric phenomenon like the roll off instability could exist. In fact, pilots try first to find a solution keeping the longitudinal flight and hesitate to escape from a crash thanks to a lateral procedure with the risk of spin.

The aim of the present study is to propose a real-time identification of deep stall entry as soon as possible and find the ad-hoc way out without knowing the aircraft aerodynamic above the stall angle. The proposed algorithm must be simple and robust because it cannot obviously be tested on a real airplane (unless on a small UAV or an aircraft designed for that purpose [27]). To avoid a false detection in normal flight condition, it would be only triggered when the aircraft would be in alternate law or in flight test phase below the stall angle. Therefore, this study concerns an actual existing aircraft but not the conception parameters involved during the design phase. In order to reach this goal, the first step is to analyze the path towards the deep stall equilibrium and the second is to identify the dynamical features of the phenomenon. The first part of the paper is about the implementation of a realistic model of a deep stall prone aircraft. The second part concerns the analysis of the aircraft model behavior applying dynamical system theory in order to have time evolution of the physical variables and modes properties near the equilibrium points. The following part proposes the real-time deep stall detection algorithm. Finally, the real-time detection is successfully applied and some recovery procedures are evaluated.

III. Aircraft model

A. Governing equations

As it is considered classically, it is assumed here that aircraft motion is longitudinal during deep stall phenomenon. In the longitudinal plane, the earth, aerodynamic and aircraft frames of reference are denoted $(\mathbf{x_0}, \mathbf{z_0})$, $(\mathbf{x_a}, \mathbf{z_a})$ and $(\mathbf{x_b}, \mathbf{z_b})$, respectively. In consequence, the nonlinear governing equations of the aircraft are in the aerodynamic frame for

the forces and the aircraft frame for the moment (see the nomenclature for the list of the symbol definitions):

$$\dot{V} = -\frac{\rho V^2 S}{2m} C_D(\alpha, q, \delta_e, \delta_f) + \frac{T(\rho, \delta_T)}{m} \cos\alpha - g \sin\gamma \tag{1}$$

$$\dot{\gamma} = \frac{\rho V S}{2m} C_L(\alpha, q, \delta_e, \delta_f) + \frac{T(\rho, \delta_T)}{mV} \sin\alpha - \frac{g}{V} \cos\gamma \tag{2}$$

$$\dot{\alpha} = q - \frac{\rho V S}{2m} C_L(\alpha, q, \delta_e, \delta_f) - \frac{T(\rho, \delta_T)}{mV} \sin\alpha + \frac{g}{V} \cos\gamma \tag{3}$$

$$\dot{q} = \frac{\rho V^2 S c}{2I_y} C_m(\alpha, q, \delta_e, \delta_f) \tag{4}$$

$$\dot{h} = V \sin\gamma \tag{5}$$

where it is assumed that thrust does not create any moment and is aligned with the $\mathbf{x_b}$ direction.

This mathematical model of longitudinal flight dynamics can be rewritten in the state space form:

$$\dot{\mathbf{X}} = f(\mathbf{X}, \mathbf{U}) \tag{6}$$

where the state vector $\mathbf{X}$ and the control vector $\mathbf{U}$ are:

$$\mathbf{X} = (V, \gamma, \alpha, q, h) \quad ; \quad \mathbf{U} = \left(\delta_e, \delta_T, \delta_f\right) \tag{7}$$

Hereafter, computation of Eqs. 1-5 is called full model and computation of only Eqs. 3-4 is called reduced model.

B. Aerodynamic coefficients

For the deep stall study, it is necessary to find realistic aerodynamic coefficients at very high AoA of a deep stall prone aircraft. These data are easier to find for a fighter aircraft in literature [14, 28] than for a transport aircraft. Nevertheless, the Learjet 23 D is a good candidate, because it was a well known deep stall prone aircraft and because Soderman and Aiken have obtained the static aerodynamic coefficients during full scale wind-tunnel tests [29]. In consequence, all static coefficients C_L, C_D and $C_{m_{static}}$ (for $q = 0$) were digitized hereafter. These experimental measurements have been interpolated with spline functions in the experimental data range and extrapolated linearly outside the bounds. Figures 1a and 1b give the lift C_L and drag C_D coefficients for a large range of AoA, respectively without flaps ($\delta_f = 0°$) and with full flaps ($\delta_f = 40°$) configurations and extreme elevator deflection angle values. Figure 1c gives $C_{m_{static}}$ for the same configurations at wing quarter chord.

The static part of the pitching moment allows to determine the AoA values at equilibrium (Fig. 1c). From the flight dynamics point of view, deep stall occurs when there exists a stable equilibrium at high AoA for a given elevator deflection angle, center of gravity and configuration (flaps up/down, etc). A longitudinal equilibrium requires, among others, a zero pitching moment and is statically stable when the α-slope of the pitching moment coefficient is negative (i.e. $\partial C_m / \partial \alpha < 0$) [30].

Moreover, the loss of tail efficiency in deep stall also affects the pitch rate derivative of the pitching moment coefficient ($\partial C_m / \partial q$). Indeed the lift of the horizontal tail creates normally an opposite moment to the aircraft pitch motion, followed by a modification of the local AoA of the tail versus that of the wing. But this effect is reduced with the degraded aerodynamics of the horizontal tail, when it is inside the separated wake of the stalled main wing. Here, a simple continuous piecewise linear function is proposed for the pitch rate derivative inspired from the model of Montgomery and Moul [31] and whose absolute value is reduced in the deep stall conditions:

$$\frac{\partial C_m}{\partial q} = \frac{C_{m_q} c}{V} \qquad \text{where} \qquad C_{m_q} = \begin{cases} -9.4 & \alpha \notin [20°, 50°] \\ 0.61 \times (\alpha - 20) - 9.4 & \alpha \in [20°, 35°] \\ -0.61 \times (\alpha - 35) - 0.25 & \alpha \in [35°, 50°] \end{cases} \tag{8}$$

It should be noticed that recent experimental studies on SUPRA aircraft project showed that the C_{m_q} increase could be higher than the one proposed in Montgomery and Moul [32, 33]. The overall aircraft pitching moment takes the following form with its diverse contributions, that is to say the quarter chord pitching moment $C_{m_{\text{static}}}$, the static margin δ_{sm} and the pitch damping C_{m_q}:

$$C_m\left(\alpha, q, \delta_e, \delta_f\right) = C_{m_{\text{static}}}\left(\alpha, \delta_e, \delta_f\right) + C_L(\alpha, \delta_e, \delta_f)\delta_{sm} + \frac{c}{V} C_{m_q}(\alpha) q \tag{9}$$

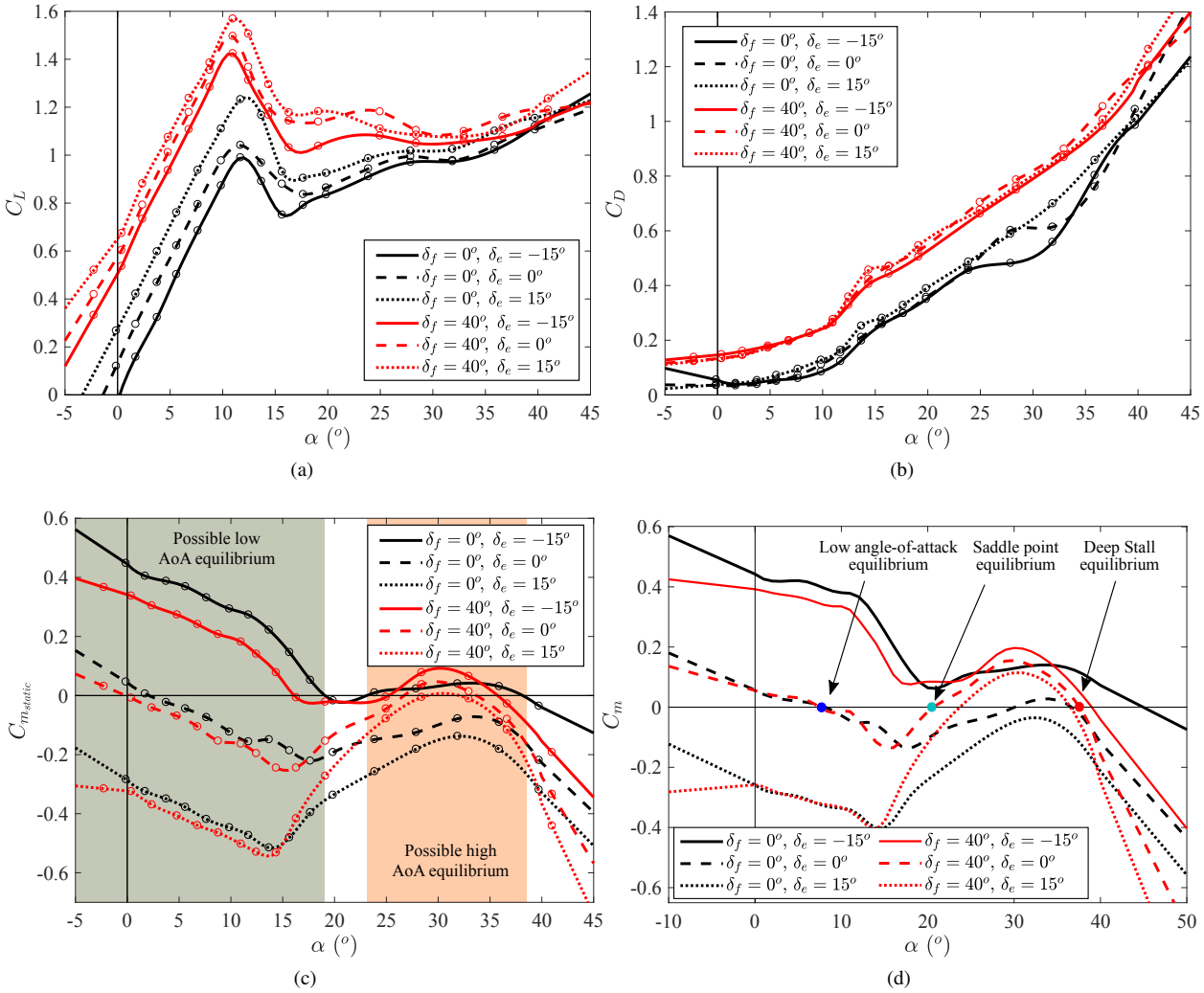

Figure 1 Interpolated static aerodynamic model from the NASA full scale Learjet 23D wind tunnel tests for various elevator commands and two flap configurations [29] : a) C_L , b) C_D , c) $C_{m_{static}}$ at wing quarter chord ("o" markers corresponds to NASA experimental measurements) d) C_m for $q = 0$ and $\delta_{sm} = -10\%$.

with

$$\delta_{sm} = \frac{x_{cg} - x_{ac}}{c} \tag{10}$$

where x_{cg} and x_{ac} are the algebraic position of the center of gravity and the wing aerodynamic center as in [29]. With this definition, the static margin is negative for an aft center of gravity. The aircraft pitching moment is given for $q = 0$ and $\delta_{sm} = -10\%$ in Fig. 1d.

Thrust in Newtons is defined using the following expression:

$$T = 26243.2(\frac{\rho}{1.225})^{0.7}\delta_T$$

where $\delta_T \in [0, 1]$. The other aircraft data are: $m = 4\,536$ kg, $I_y = 33940.7$ kg m^2, $c = 2.14$ m and $S = 21.48$ m^2 [29, 34]. The thrust contribution on the aircraft pitching moment is neglected hereafter. It can be noted that for a T-tail aircraft with engines on the rear fuselage, the moment is significantly smaller than in a conventional setup where the engines are placed under the wings. Finally, it is assumed as usual that $\partial C_L/\partial q = \partial C_D/\partial q = 0$.

IV. Analysis of aircraft model behavior

In this part, characteristics properties of the aircraft dynamics near deep stall are identified in order to predict the convergence of its trajectory in a phase portrait toward a low or a high AoA equilibrium.

A. General aircraft dynamics

An aircraft may meet deep stall for several ranges of elevator deflection angles in a given configuration (static margin, flaps, etc.). For such critical cases, there are three equilibria for one fixed elevator deflection angle δ_e. They correspond to the AoA for which the overall pitching moment is equal to zero ($C_m(\alpha, \delta_e) = 0$ on Fig. 1c for $\delta_{sm} = 0\%$ and on Fig. 1d for $\delta_{sm} = -10\%$). These equilibria are: the classical low AoA equilibrium, an unstable equilibrium at medium AoA (called saddle point) and the stable equilibrium at high AoA associated to deep stall. These points are marked by color dots for $\delta_f = 40°$ and $\delta_e = 0°$ in Fig. 1d.

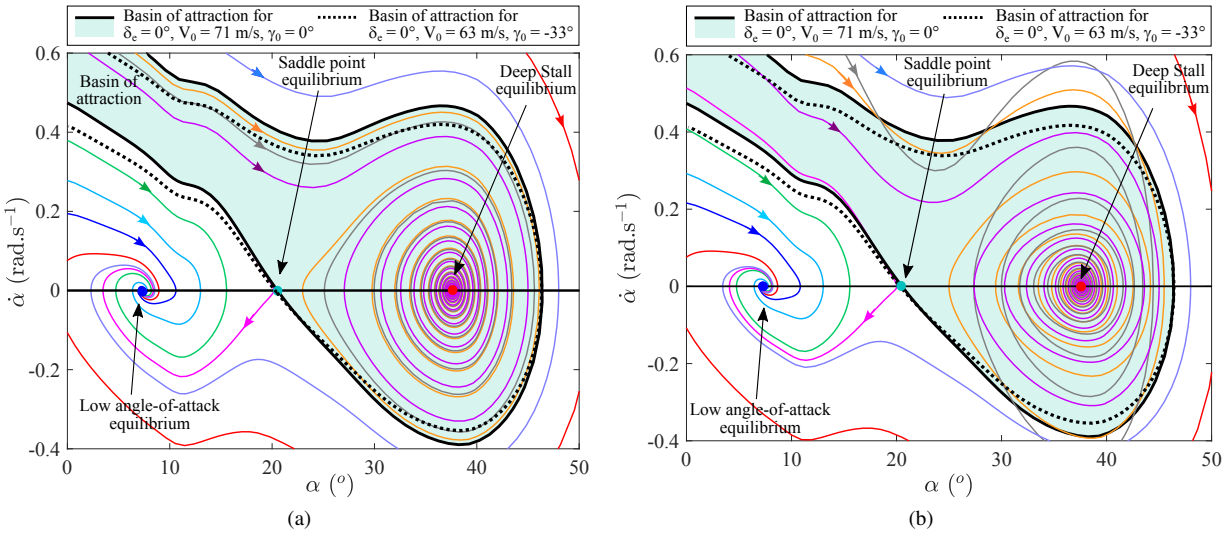

Figure 2 Phase portrait comparison of the two models for flight dynamics computation of the Learjet 23D model: a) reduced model, b) full model and basin of attraction of the reduced model (flaps down $\delta_f = 40°$, $\delta_e = 0°$, $\delta_T = 0.4$ and $\delta_{sm} = -10\%$ with initial conditions $V_0 = 71$ m/s, $\gamma_0 = 0°$, $\alpha_0 = 0°, 5°, 10°, 13°, 20°, 23°, 30°, 45°, 48°$, $q_0 = 0$ rad/s and $h_0 = 6000$ m).

Figure 2a and 2b show the phase portrait of the Learjet 23D, typical of a deep stall prone aircraft, computed with the reduced model and the full model, respectively. A stable manifold can be computed with the reduced model (thick black curve in Fig. 2a), it starts from the saddle point and delimits the basin of attraction of the equilibrium at high AoA. Note that the stable manifold is computed using a backward time integration starting from a point in the neighborhood of the saddle point. Two types of behaviors can be distinguished in Fig 2a. First, when the airplane converges towards a stable equilibrium point, the distance between two angles-of-attack for which $\dot{\alpha} = 0$ becomes more and more reduced. Secondly, in the neighborhood of the saddle point, all the trajectories are attracted by this equilibrium and then repelled from it. The trajectories remaining at the right of the saddle point equilibrium stay in the basin of attraction as shown by several authors [14, 31, 35]. Other trajectories (outside the basin of attraction) converge towards the low AoA equilibrium. Another simple remark never pointed out in previous studies, to the best of our knowledge, is the way of convergence toward a stable equilibrium. Figure 2a shows a fast convergence of the short-period mode to the low AoA in only one cycle while the convergence to the high AoA is slow and takes many cycles. Slow convergence can be considered like an opportunity allowing sufficient time to initiate the recovery procedure. This difference is explained by the large difference in damping for the two cases that will be explained and quantified in part IV.C.

Another point is that the reduced model computations are carried out with the hypotheses of constant slope and velocity. For the low AoA equilibrium, the slope is necessarily null, corresponding to the light green basin of attraction. On the contrary, for the high AoA equilibrium, the aircraft gets a very negative slope. For the studied configuration, the airplane is on a -33° slope and its velocity is decreased to 63 m/s. These conditions give a new stable line (dotted black

in Fig. 2a) and a new basin of attraction. It can be noticed that both basins of attraction are very close. Finally the slope has little influence on the airplane behavior. Hereafter, only the basin of attraction for a slope equal to zero is considered since this is the one indicating whether or not the airplane is entering in deep stall. A second point is that the basin of attraction can be plotted only for the reduced model, because only the planar case insures that the trajectories are not crossing each others [31, 36]. This is what Fig. 2b shows, where the full model is considered. Then, it can be noticed that the basins of attraction previously computed provide a blurred criterion for the convergence or divergence toward the high AoA equilibrium.

Fig. 3 presents an airplane at low AoA equilibrium whose pilot applies a pitch-up command during 1s followed by a return to $\delta_e = 0$. In this realistic airplane flight with a change on pilot command, the basin of attraction computed with the reduced model provides a good estimate of the final equilibrium for both the reduced and full calculations. In addition, the basin of attraction for a full pitch-down command is plotted in the figures (in light red), showing that there is no possible recovery of the airplane after one cycle.

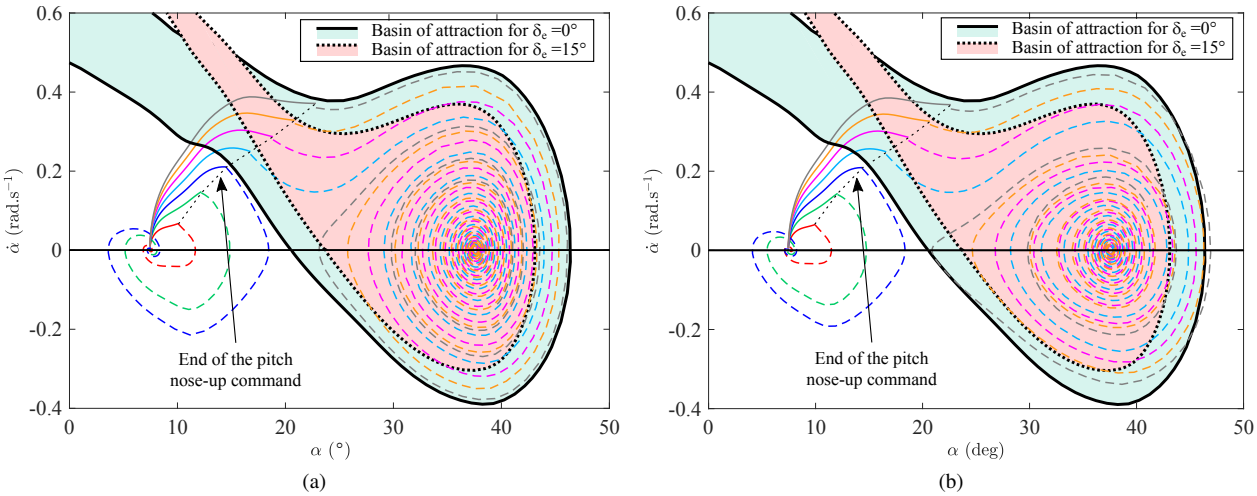

Figure 3 Phase portrait comparison of two various model for flight dynamics computation of the Learjet 23D model starting from equilibrium and applying various pitch nose-up command during 1s: a) reduced model with basin of attraction, b) full model with reduced model basin of attraction (flaps down $\delta_f = 40°$, $\delta_T = 0.4$ and $\delta_{sm} = -10\%$ with initial conditions $\delta_{e_{init}} = \{-3, -5, -7, -9, -11, -13, -15\}°$, $V_0 = 71$ m/s, $\gamma_0 = 0°$, $\alpha_0 = 7.45°$, $q_0 = 0$ rad/s and $h_0 = 6000$ m).

Figure 4 presents the bifurcation diagram corresponding to the AoA at equilibrium as a function of the elevator position δ_e. It shows two limit points (LP), also called saddle-node bifurcations or fold bifurcation, at $\delta_e = -10°$ and $\delta_e = 5°$ delimiting three zones [36]. For an elevator deflection angle below $-10°$ and above $5°$, there is only one stable equilibrium. For an elevator deflection angle between $-10°$ and $5°$, there are three equilibria, two stable ones and an unstable one. Near an elevator deflection angle of $\delta_e \approx -10°$ in a stabilized situation at low AoA, a pitch-up command can produce a jump to the stable branch at high AoA which will not be so easy to recover from since a reverse pitch-down command may change the equilibrium state value, but the aircraft may remain at high AoA. There is a phenomenon which looks like an hysteresis. It is a hazardous situation and as long as the aircraft is on the stable branch at low AoA, the pilot may expect and foresee the happening of change of AoA leading to deep stall.

B. Effect of altitude, velocity, flaps and pitch damper

The basins of attraction for diverse configurations of the Learjet 23 D are now compared.

Figure 5a shows the basin of attraction with flaps up for various altitudes between 3000 m and 10000 m. The deep stall basin of attraction is rather limited. The altitude has little influence on its extension around the high AoA equilibrium point. However, the branch at the left top corner is influenced by the altitude. It means that the AoA for which the aircraft can enter into the basin of attraction (Fig. 3) is lower at high altitude ($h = 10000$ m). Figure 5b shows the basin of attraction with flaps down for the same altitudes but for a slightly lower speed corresponding to the maximum speed the flaps down configuration can bear. Larger basins of attraction are observed, showing that this

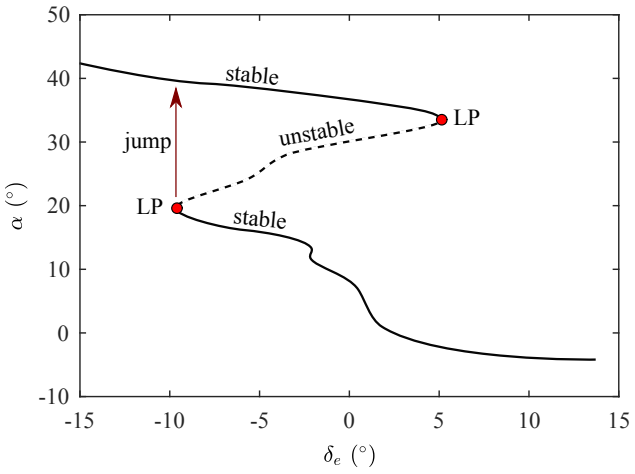

Figure 4 Example of a bifurcation diagram (α, δ_e) of the Learjet 23D model (flaps up $\delta_f = 0°$, $\delta_{sm} = -10\%$).

configuration is more deep stall prone. As a consequence, it is advisable to retract the flaps when a situation prone to deep stall is detected for this type of T-tail aircraft.

Figure 5c shows the basin of attraction with flaps up for various velocities between 80 m/s and 160 m/s at $h = 6000$ m. The velocity has little influence on the basin of attraction except for 80 m/s which corresponds to the region of the reversed command of the power curve.

Effects of pitch damping on the aircraft behavior have been widely studied in the past by Thomas and Collingbourne [35]. Figure 5d shows the basin of attraction with pitch damper for various altitudes between 3000 m and 10000 m and a velocity of 80 m/s. The basin of attraction is larger when the pitch damper is engaged (comparison with Fig. 5b). Thus, it can be advised to switch off the pitch damper when a situation prone to deep stall is detected. This effect can be explained by the design of a pitch damper: a component of elevator deflection angle δ_e which is added to the pilot action and proportional to the pitch rate q. It produces more pitch damping which is translated mathematically into a more negative derivative of the pitching moment coefficient with respect to the dimensionless pitch rate C_{m_q}. Moreover, since the oscillations are less damped out and the divergence of the vector field is lower when the pitch damper is switched off, the aircraft is less likely to converge towards the deep stall equilibrium and since the damping of the movement is lower, the pilot has a little more time available to react.

C. Short-period mode properties at low and high AoA

The relatively fast motion observed in Fig. 2a corresponds to short-period modes. These modes are classically assumed decoupled with phugoid modes at low AoA [30, 37] but also here at high AoA [38]. Note that the simulations of the reduced model seem quite close to the ones of the full model (Fig. 3).

By linearizing the dynamics of the lift and pitch equations near a low AoA equilibrium for a fixed airspeed V_e, altitude and angle-of-attack α_e, analytical expressions of the pulsation ω_{spm} and of the damping ζ_{spm} can be obtained classically for the short-period mode [30, 37]:

$$\omega_{spm}^2 = -\frac{V_e^2 \rho c S}{2I_y}\left[\left(\frac{\rho S V_e}{2m}C_{L_\alpha} + \frac{T}{mV_e}\right)\frac{c}{V_e}C_{m_q} + C_{m_\alpha}\right] \tag{11}$$

$$2\zeta_{spm}\omega_{spm} = \frac{\rho S V_e}{2m}C_{L_\alpha} - \frac{c^2 \rho S V_e}{2I_y}C_{m_q} + \frac{T}{mV_e} \tag{12}$$

where C_{L_α}, C_{m_α} and $C_{m_q} = (V_e/c) \times \partial C_m / \partial q$ are computed for the values: $\alpha = \alpha_e$, $q = 0$, δ_e and δ_f. It can be shown that a quasi-similar expression can be obtained in the case of high AoA [38]:

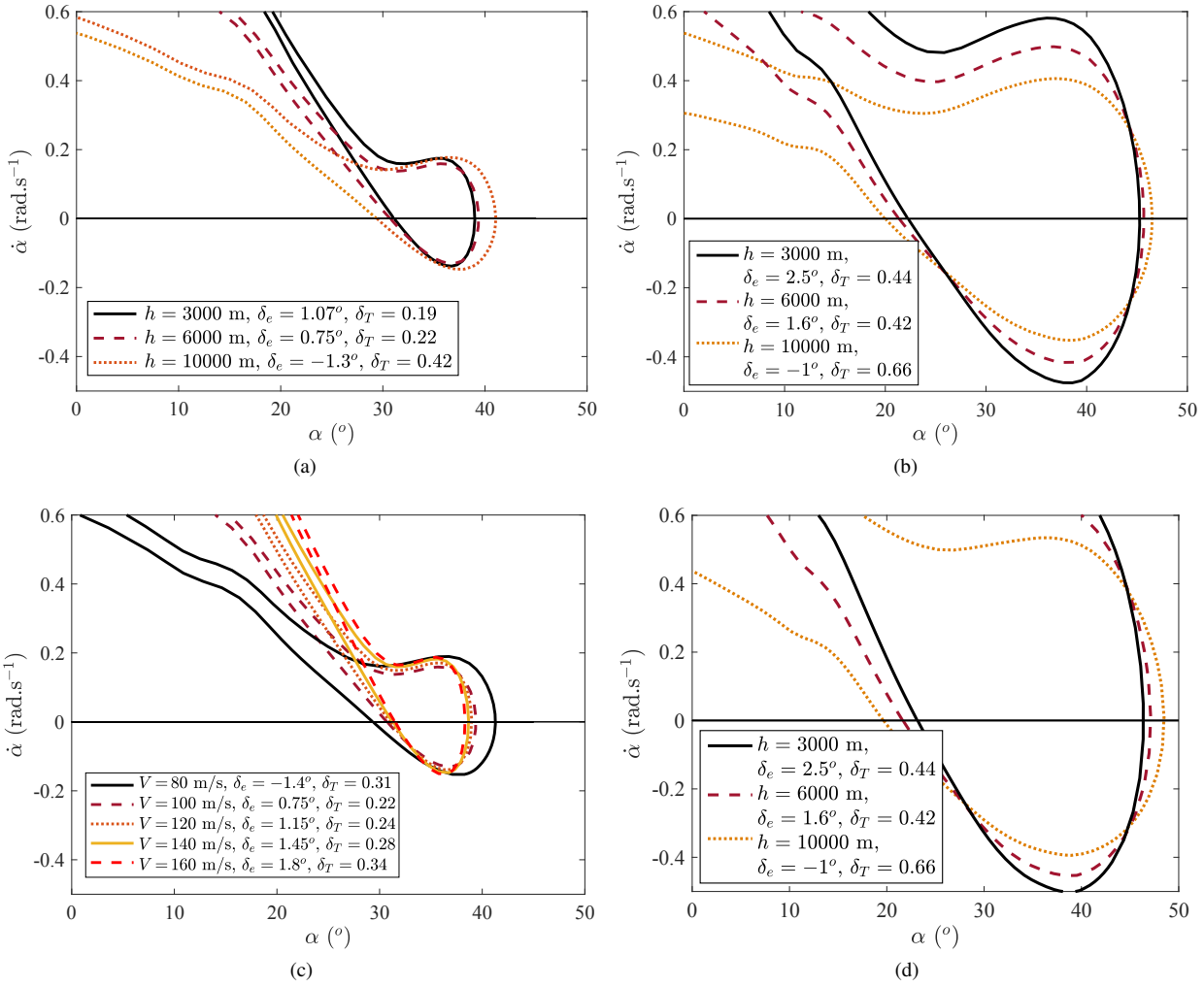

Figure 5 Comparison of the basins of attraction for different configurations of the Learjet 23D model ($\delta_{sm} = -10\%$, $\gamma_0 = 0°$, $q_0 = 0$ rad/s): a) flaps up for various altitude h for $V = 100$ m/s b) flaps down for various altitude h for $V = 80$ m/s, c) flaps up for various velocities V for $h = 6000$ m, d) flaps down with pitch damper for various altitude h for $V = 80$ m/s.

Table 1 Short-period mode approximation for the Learjet 23D at low and high AoA (flaps down $\delta_f = 40°$, $\delta_{sm} = 0\%$).

Parameters	Units	Low AoA	High AoA
α_e	deg	4.4	34.2
δ_e	deg	-3	-3
δ_T	-	0.48	1
V_e	m/s	78.3	64.9
h	km	4	4
λ	-	$-0.789 \pm 1.39i$	$-0.0762 \pm 1.69i$
ω_{spm}	rad/s	1.60	1.69
ζ_{spm}	-	0.49	0.045

$$\omega_{spm}^2 = -\frac{V_e^2 \rho c S}{2I_y}\left[\left(\frac{\rho S V_e}{2m}C_{L_\alpha} + \frac{T}{mV_e}\cos\alpha_e\right)\frac{c}{V_e}C_{m_q} + C_{m_\alpha}\right] \quad (13)$$

$$2\zeta_{spm}\omega_{spm} = \frac{\rho S V_e}{2m}C_{L_\alpha} - \frac{c^2 \rho S V_e}{2I_y}C_{m_q} + \frac{T}{mV_e}\cos\alpha_e \quad (14)$$

but the values of derivatives C_{L_α}, C_{m_q} are very different because they are measured near α_e which is very large in this case.

Table 1 shows an example of short-period mode computation for the Learjet 23 D with the Eqs. 11-14. This numerical application shows clearly that the damping of the short-period mode is far smaller at high AoA than at low AoA (approximately 10 times smaller). This phenomena can be explained by the fact that in stall, the lift curve slope C_{L_α} is lower (see for example the slope of C_L between 15° and 40° vs. the slope at origin on Fig. 1a which is largely reduced or even negative). Moreover, the absolute value of the pitching moment coefficient derivative ($\left|C_{m_q}\right|$) is also clearly reduced (see C_{m_q} definition in the part III.B). On the other hand, the pulsation is quite the same at low or high AoA and cannot be used as a discriminant condition to find the type of equilibrium. Note also that the period of the short-period mode at high AoA is approximately equal to 4 s allowing to confirm that the convergence to the deep stall equilibrium is relatively slow and the order of magnitude is around one minute (see Fig. 2a).

V. Real-time deep stall detection

Previous main remarks are now used to propose a fast detection algorithm of deep stall without knowing the aircraft aerodynamics at medium and high AoA. The fast detection permits, among others, to have a sufficient level of energy to go out from deep stall and to react as early as possible, as far as possible from the deep stall equilibrium. The main idea of this algorithm is to predict the evolution of the aircraft trajectory in the $(\alpha, \dot{\alpha})$ phase portrait using the relative positions of the extrema.

Some assumptions should be made before describing the method. Firstly, it is assumed that α and $\dot{\alpha}$ (or q) are measured in real-time with sufficient confidence up to very high AoA. Even if the data are noisy, it is also assumed that a standard filter allows to obtain sufficiently smooth estimation of these data. Secondly, the aircraft is assumed free and in a quasi longitudinal flight (quasi-symmetric aircraft motions in the vertical plane). Free means that the pilot makes no supplementary action to the pitch command during detection.

To avoid a false detection in normal flight condition, the algorithm is started only when α exceeds α_{stall} but a different choice can be made. Starting from the stall angle, Fig. 6 shows two typical trajectories. The first one converges to a low AoA and the second one to a high AoA. As it was said before, in the two cases, the aircraft is repelled from the saddle point equilibrium. On the figures, α is incrementally denoted α_i ($i \in \mathbb{N}^*$) when $\dot{\alpha} = 0$ and α_{dj} ($j \in \mathbb{N}^*$) when $d\dot{\alpha}/d\alpha = 0$. From a mathematical point of view, the main difference between the portraits of Figs. 6a and 6b is the number of α_{dj} between two successive α_i (α_1 and α_2 in the figures). Consequently, the case of the convergence to a low AoA (Fig 6a) can be easily eliminated with the condition $\max(j) = 1$. In the second case (Fig 6b) and if $\alpha_{d1} \in]\alpha_2, \alpha_1[$, aircraft begins to describe a spiral trajectory typical of deep stall. Another step is then necessary to confirm this spiral

trajectory and the convergence into a high AoA. The analysis of what happens between α_2 and α_3 can confirm this fact. If there is again only one α_{dj} (α_{d2} in Fig. 6b) i.e. $\max(j) = 2$ and $\alpha_{d2} \in]\alpha_2, \alpha_3[$ and also $\alpha_3 \in]\alpha_2, \alpha_1[$, the detection of a high AoA equilibrium is more and more probable. Then, an approximation of the AoA at equilibrium and the damping value of the short-period mode can be computed with the mean and the half-cycle turning points approximation formulae:

$$\alpha_e = \frac{\alpha_{d1} + \alpha_{d2}}{2} \tag{15}$$

$$\zeta_{spm} = \frac{1}{2\pi} \ln\left(\frac{\alpha_1 - \alpha_2}{\alpha_3 - \alpha_2}\right) \tag{16}$$

Finally, the detection is considered true if $\alpha_e \gg \alpha_{stall}$ and $\zeta_{spm} \ll \zeta_{spm}^{LAoA}$. The identification algorithm is summarized in Fig. 7. Note that the algorithm distinguishes different extrema order if $\alpha_1 > \alpha_2$ or $\alpha_1 < \alpha_2$. Another remark is that the algorithm is written with the $(\alpha, \dot{\alpha})$ state values but it could also have been done with the (α, q) system. The last comment is that other kinds of trajectories in the $(\alpha, \dot{\alpha})$ portrait can be found in the literature [35, 39]. However, it has been checked that any other trajectory than spiral is rejected by the present simple algorithm.

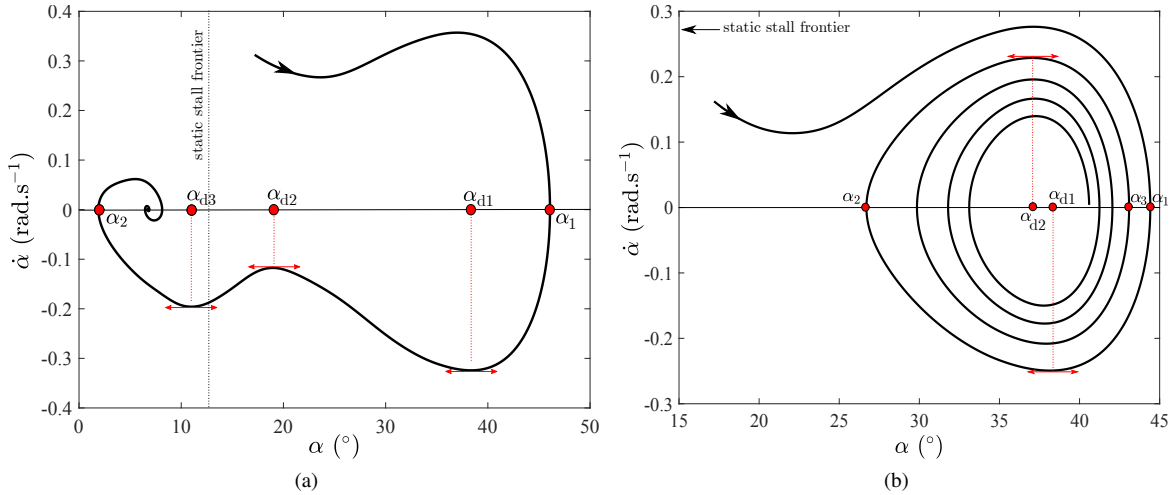

Figure 6 Definition of α_i and α_{dj} for typical paths in the phase portrait at high AoA of the Learjet 23D model: a) convergence towards an equilibrium at low AoA, b) convergence towards an equilibrium at high AoA. (reduced model, flaps down $\delta_f = 40°$, $\delta_e = 0°$, $\delta_T = 1$ and $\delta_{sm} = -10\%$ with initial conditions $V_0 = 72$ m/s, $\gamma_0 = 0°$, $\alpha_0 = 44°$, 46°, $q_0 = 0$ rad/s and $h_0 = 10\,000$ m).

VI. Application of the real-time detection algorithm and recovery procedure

In this section, the prediction algorithm is applied on the aircraft model and recovery is performed with a full pitch-down command applied manually or automatically.

In the past, Thomas and Collingbourne [35] carried out a large numerical study to identify the entry and exit maneuvers for a deep stall prone aircraft and noticed a strong influence of initial conditions. Figure 8 shows two kinds of pilot's reaction for an airplane in the deep stall basin of attraction. In Fig. 8a, the pilot is supposed to understand the airplane deep stall after 40 s and applies a full pitch down command of $\delta_e = 15°$. This is corresponding to an estimated reaction time necessary to understand this unusual flight situation. He does not succeed in going out from the deep stall equilibrium because, after 40s, the position in the phase portrait is completely inside the rose basin of attraction corresponding to $\delta_e = 15°$. The aircraft reaches a new deep stall equilibrium with a little lower AoA. In Fig. 8b, the pilot is warned of a fore-coming deep stall by the algorithm (starting from the initial point of the simulation) after approximately 5 s and reacts 5 s later by applying a large pitch-down command of $\delta_e = 15°$ during 5 more seconds and then release the command. This pilot succeeds in going out from deep stall and reaches a low AoA. This example shows the usefulness of being aware of the dangerous situation as early as possible but it is not sufficient. The next two

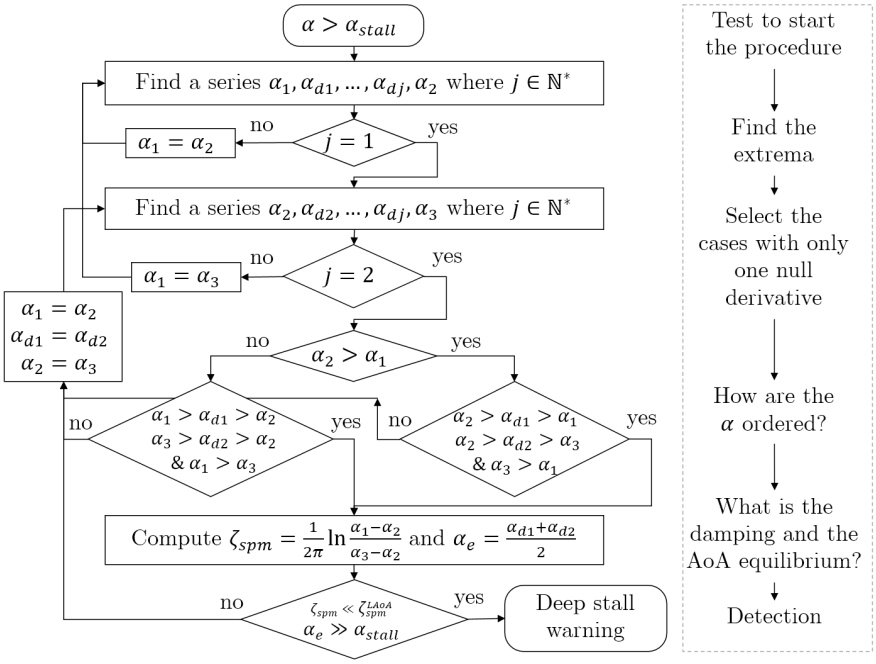

Figure 7 Real-time algorithm for deep stall prediction.

examples in Fig. 9 show that the time instant when the pitch-down command is applied is as well as important. In the first case (Fig. 9a), the pilot applies the command just after that the AoA reaches the first turning point α_4, that is to say when both α and $\dot{\alpha}$ decrease. In this case, the pilot succeeds in going out from deep stall. In the second case (Fig. 9b), the pilot applies the command just after that the AoA reaches the second turning point α_5, that is when both α and $\dot{\alpha}$ increase. The pilot does not succeed in coming back to a low AoA even if the command is maintained during 10 s.

The last example shows that, in order to avoid the basin of attraction ($\delta_e = 15°$) where deep stall recovery is impossible, it is better to apply a pitch-down command when both α and $\dot{\alpha}$ decrease. In order to justify this statement, a simplified model for the short-period mode is written in the following form (ignoring the term with C_{L_α}):

$$\dot{\alpha} = q \tag{17}$$

$$\dot{q} = \frac{\rho V^2 S c}{2 I_y} \left(C_{m_{static}}(\alpha, \delta_e) + \frac{c}{2V} C_{m_q}(\alpha)\, q \right) \tag{18}$$

with $C_{m_q}(\alpha) < 0$ and $dC_{m_{static}}/d\delta_e < 0$. When applying a pitch-down command ($\delta_e > 0$), the variation of the pitching moment is negative $\Delta C_{m_{static}}(\alpha, \delta_e) < 0$. Thus the pitch rate derivative $\dot{q}$ is more negative and the pitch rate decreases even more. In order to be in a situation where the AoA reduces much more and such that it flies easier towards lower AoA, it is necessary that both derivatives of AoA and of pitch rate are negative, which means that both variables α and q decrease. This case is shown in Fig. 9a.

This part demonstrates the interest of the detection algorithm but also that the choice of the time instant when the pitch-down command is applied is fundamental to recover the aircraft. Because it is not possible to expect the pilot to apply the command at the right time instant, it can be concluded that the success of the recovery necessitates to automate this last step. It consists simply in applying the larger pitch-down command when α_3 or α_4 is reached, depending on the order of α_i and until α_{stall} threshold is crossed. The basic recovery algorithm is summarized in Fig. 10.

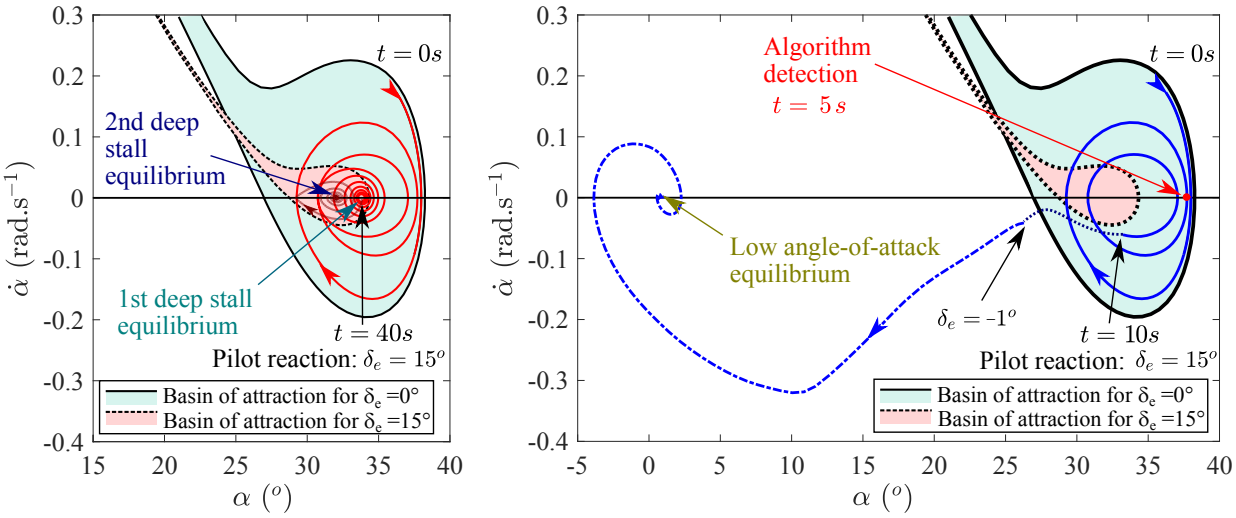

(a) Pilot's time reaction = 40s

(b) Pilot's time reaction = 10s

Figure 8 Comparison of pilot's correcting action near deep stall equilibrium: a) without algorithm detection leading to a failed recovery, b) with algorithm detection leading to a successful recovery (full model, flaps down $\delta_f = 40°$, $\delta_e = 0°$, $\delta_T = 0.4$ and $\delta_{sm} = 0\%$ with initial conditions $V_0 = 100$ m/s, $\gamma_0 = 0°$, $\alpha_0 = 37.5°$, $q_0 = 0$ rad/s and $h_0 = 6000$ m).

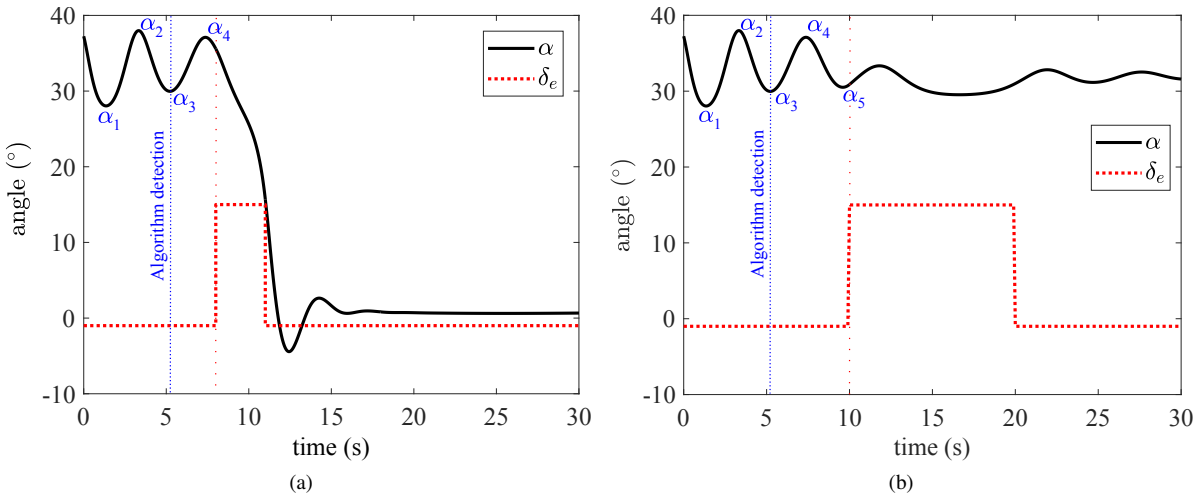

(a)

(b)

Figure 9 Pitch-down maneuvers for recovery after deep stall detection: a) maneuver after α_4 leading to a successful recovery, b) maneuver after α_5 leading to a failed recovery (full model, flaps down $\delta_f = 40°$, $\delta_e = 0°$, $\delta_T = 0.4$ and $\delta_{sm} = 0\%$ with initial conditions $V_0 = 100$ m/s, $\gamma_0 = 0°$, $\alpha_0 = 37.5°$, $q_0 = 0$ rad/s and $h_0 = 6000$ m).

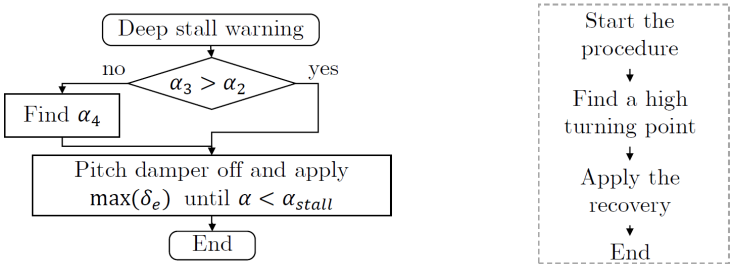

Figure 10 Real-time algorithm for recovery from deep stall.

In order to validate the detection and recovery algorithm for different initial conditions, simulations have been done for three aircraft configurations (aft CG and flap up, neutral CG and flap down, aft CG and flap down) with the reduced model or the full model in Fig. 11. The procedure is the same as in Fig. 3 but the detection and recovery algorithms are now applied. Both models (reduced and full) provide similar behaviors. Simulations show that there exist three kind of situation for the detection algorithms:

- Figs. 11a-11b. With flap up and a static margin of -10%, C_m curve has only one equilibrium at low AoA for full pitch down (Fig. 1d, black dotted line, $\delta_e = 15°$). In this case, even if the aircraft goes into deep stall, the tail command is sufficiently effective to recover at any time. This is shown with the basin of attraction which disappear for higher command than $\delta_e = 5°$ (a small basin of attraction is plotted for $\delta_e = 5°$). Then, the algorithm is always efficient and the time instant for applying recovery procedure has no influence on the success of the procedure.
- Figs. 11c-11d. With flap down and a static margin of 0%, C_m curve has a deep stall equilibrium for full pitch down (Fig. 1c, red dotted line, $\delta_e = 15°$). In this case, when the aircraft goes into deep stall, the tail command can be ineffective to recover. The basin of attraction exists for $\delta_e = 15°$ but is much smaller than the case where $\delta_e = 0°$. The algorithm is always efficient. The time instant for applying recovery procedure is important because the trajectory of the aircraft in the phase portrait can cross the basin of attraction for $\delta_e = 15°$. In this case, it seems to be adapted to apply the full pitch-down command far from this new basin.
- Figs. 11e-11f. With flap down and a static margin of -10%, C_m curve has a deep stall equilibrium for full pitch-down (Fig. 1d, red dotted line, $\delta_e = 15°$) and a large part of this curve is above the abscissa axis. In this case, when the aircraft goes into deep stall, the tail command can be highly ineffective to recover. The basin of attraction for $\delta_e = 15°$ is very large. After approximately one cycle the aircraft is in this new basin of attraction and a full pitch-down command is ineffective. The algorithm is efficient for only two cases (orange and gray curves). It can be noticed that the time instant for applying recovery procedure is necessarily at the right of the basin of attraction for $\delta_e = 15°$.

In the last two cases, it is always possible to recover from deep stall by retracting the flaps to return to the first situation (Figs. 11a-11b). But retracting flaps is not always possible in particular during hazardous situations.

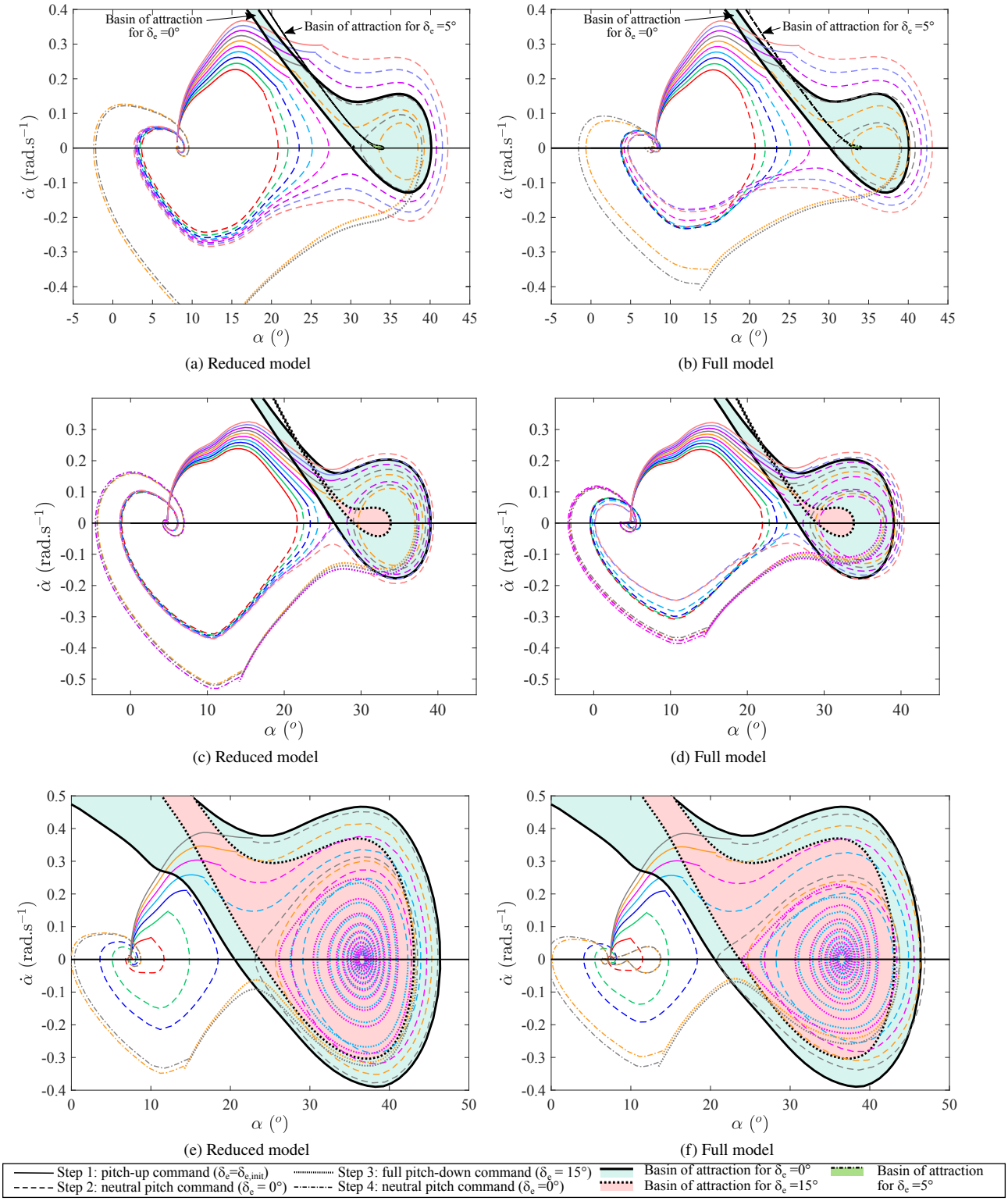

Figure 11 Automatic detection and recovery of the Learjet 23D model for various configurations and static margins ($\gamma_0 = 0°$, $q_0 = 0$ **rad.s**$^{-1}$, $h_0 = 6000$ **m**)**: a-b) flaps up,** $\delta_{sm} = -10\%$, $\delta_T = 0.4$, $V_0 = 83$ **m.s**$^{-1}$, $\alpha_0 = 8.1°$, $\delta_{e_{\text{init}}} = \{-6, -6.5, \ldots -10.5\}°$**, c-d) flaps down,** $\delta_{sm} = 0\%$, $\delta_T = 0.48$, $V_0 = 78.3$ **m.s**$^{-1}$, $\alpha_0 = 4.8°$, $\delta_{e_{\text{init}}} = \{-12, -12.3, \ldots -14.7\}°$**, e-f) flaps down,** $\delta_{sm} = -10\%$, $\delta_T = 0.42$, $V_0 = 71$ **m.s**$^{-1}$, $\alpha_0 = 7.45°$, $\delta_{e_{\text{init}}} = \{-3, -5, \ldots -15\}°$**.**

VII. Conclusion

This study about the loss-of-control of an airplane in deep stall shows that a recovery could be possible in real-time using a simple algorithm for detection and recovery. To reach this goal, the first part is concerned with the analysis of deep stall in a flight dynamics point of view in order to obtain its main properties. This was done with a Learjet 23D aircraft model and non linear dynamic analysis. This analysis pointed out that the manner to reach a low or a high angle-of-attack (AoA) equilibrium is largely different. In the two cases, it is observed a short-period mode with quasi the same pulsation but with a ten times smaller damping for the high AoA equilibrium. It results a characteristically spiral trajectory in the phase portrait. Using that fact, an algorithm is proposed to reject the trajectories which do not have this form. Two criteria are then used to confirm the convergence toward a deep stall equilibrium. The first one is a comparison between α_{stall} and the estimated value of the AoA for this equilibrium, which should be greater. The second one is a comparison between the usual short-period mode damping at low AoA and the estimated value at this moment which should be largely smaller. Using this algorithm, several cases of recovery are studied. Recovery is very effective when the pitch command is applied at the correct time instant that is when both α and $\dot{\alpha}$ decrease. It is then proposed to fully automate the recovery procedure by applying the larger pitch-down command at the right time instant with a second very basic algorithm.

References

[1] Torenbeek, E., and Wittenberg, H., *Flight Physics: Essentials of Aeronautical Disciplines and Technology, with Historical Notes*, Springer, London, 2009, p. 396. doi:10.1007/978-1-4020-8664-9.

[2] Abzug, M., and Larrabee, E., *Airplane Stability and Control : A History of the Technologies that Made Aviation Possible*, ISBN: 0-521-80992-4, Cambridge University Press, 2008, Chap. 14, pp. 209, 212. doi:10.1017/CBO9780511607141.

[3] Roberts, L., Smith, T., Van Norman, D., and Brown, M., "Safety recommandation A-94-101," Tech. rep., National Transportation Safety Board, Washington D.C., May 1994. Https://www.ntsb.gov/safety/safety-recs/recletters/A94_101.pdf.

[4] Taylor, R., and Ray, E., "A systematic study of the factor contributing to post-stall longitudinal stability of T-Tail Transport configurations," *AIAA Aircraft Design and Technology Meeting*, Los Angeles, 1965. AIAA PAPER 65-737.

[5] Taylor, R., and Ray, E., "Deep Stall aerodynamic characteristics of T-Tail aircraft," *NASA Conference On Aircraft Operating Problems*, Vol. NASA SP-83, Washington, 1965, pp. 113–121.

[6] White, M. D., and Cooper, G. E., "Simulator studies of the deep-stall," *NASA Conference on Aircraft Operating Problems: A Compilation of Papers Presented*, Langley Research Center, 1965, p. 101.

[7] Faure, T. M., Hétru, L., and Montagnier, O., "Aerodynamic features of a two-airfoil arrangement," *Experiments in Fluids*, Vol. 58, No. 10, 2017. doi:10.1007/s0034, 146.

[8] Byrnes, A., Hensleigh, W., and Tolve, L., "Effect of horizontal stabilizer vertical location on the design of large transport Aircraft," *Journal of Aircraft*, Vol. 3, No. 2, 1966, pp. 97–104. doi:10.2514/3.43712.

[9] Kenneth, P., and Spreeman, "Design Guide for Pitch-Up Evaluation and Investigation at High Subsonic Speeds of Possible Limitations Due to Wing-Aspect-Ratio Variations," Technical Memorandum X-26, NASA, 1959.

[10] Harper, C., and Maki, R., "A Review of the Stall Characteristics of Swept Wings," Technical Note D-2373, NASA, Ames Research Center, Moffet Field, California, 1964.

[11] Iloputaife, O., "Design of a Deep Stall Protection for the C-17A," *Journal of Guidance, Control, and Dynamics*, Vol. 20, No. 4, 1997. doi:10.2514/2.4109.

[12] Wall, R., "A400M To Shed Strain Gauges That Slow Flight Testing," *Aviation week - Aerospace Daily and Defense Report*, 2010, p. 2.

[13] coll., "Final report on the accident on 1st June 2009 to the Airbus A330-203 registered F-GZCP operated by Air France flight AF 447 Rio de Janeiro–Paris," Tech. rep., Bureau d'Enquêtes et d'Analyses pour la sécurité de l'aviation civile (BEA), 2012.

[14] Goman, M., Zagainov, G., and Khramtsovsky, A., "Application of bifurcation methods to nonlinear flight dynamics problems," *Progress in Aerospace Sciences*, Vol. 33, 1997, pp. 539–586. doi:10.1016/S0376-0421(97)00001-8.

[15] Wang, P., and Shi, Z., "Study of deep-stall characteristics and longitudinal special phenomena of T-tail aircraft," *Mechatronics and Automation (ICMA), 2010 International Conference on*, IEEE, 2010, pp. 59–64. doi:10.1109/ICMA.2010.5588718.

[16] Shi, Z., and Fan, L., "Bifurcation analysis of polynomial models for longitudinal motion at high angle of attack," *Chinese Journal of Aeronautics*, Vol. 26, No. 1, 2013, pp. 151–160. doi:10.1016/j.cja.2012.12.019.

[17] Kolb, S., Hétru, L., and Faure, T., "Nonlinear analysis of the longitudinal flight dynamics of a transport airplane," *5th European Conference for Aeronautics and Space Sciences*, Munich, Germany, 2013. Paper TuA07.

[18] Hétru, L., Kolb, S., Montagnier, O., and Faure, T., "Tandem airfoil vortex interaction in deep-stall," *14th European Turbulence Conference*, Lyon, France, 2013. Paper ID–243.

[19] Xin, Q., and Shi, Z., "Bifurcation analysis and stability design for aircraft longitudinal motion with high angle of attack," *Chinese Journal of Aeronautics*, Vol. 28, No. 1, 2015, pp. 250–259. doi:10.1016/j.cja.2014.12.022.

[20] Kolb, S., Hétru, L., Faure, T. M., and Montagnier, O., "Nonlinear analysis and control of an aircraft in the neighbourhood of deep stall," *AIP Conference Proceedings*, Vol. 1798, AIP Publishing, 2017. doi:10.1063/1.4972672, 020080.

[21] Taniguchi, H., "Analysis of Deepstall Landing for UAV," *Proceedings of ICAS 2008*, Anchorage, Alaska, USA, 2008.

[22] Kubo, D., and Suzuki, S., "High angle of attack flight control of a tail-sitter unmanned aircraft," *Proceedings of ICAS 2012*, Brisbane, Australia, 2012.

[23] Mathisen, S. H., Fossen, T. I., and Johansen, T. A., "Non-linear Model Predictive Control for Guidance of a Fixed-Wing UAV in Precision Deep Stall Landing," *International Conference on Unmanned Aircraft Systems, Denver*, 2015.

[24] Richards, N. D., Gandhi, N., Bateman, A. J., Klyde, D. H., and Lampton, A. K., "Vehicle Upset Detection and Recovery for Onboard Guidance and Control," *Journal of Guidance, Control, and Dynamics*, 2016, pp. 1–14. doi:10.2514/1.G001738.

[25] Lombaerts, T., Schuet, S., Acosta, D., Kaneshige, J., Shish, K., and Martin, L., "Piloted Simulator Evaluation of Safe Flight Envelope Display Indicators for Loss of Control Avoidance," *Journal of Guidance, Control, and Dynamics*, Vol. 40, No. 4, 2016, pp. 948–963. doi:10.2514/1.G001740.

[26] Lombaerts, T., Looye, G., Ellerbroek, J., and Rodriguez y Martin, M., "Design and piloted simulator evaluation of adaptive safe flight envelope protection algorithm," *Journal of Guidance, Control, and Dynamics*, 2017, pp. 1–23. doi:10.2514/1.G002525.

[27] Sim, A. G., "Flight characteristics of a manned, low-speed, controlled deep stall vehicle," *11th Atmospheric Flight Mechanics Conference*, Seattle, USA, 1984. doi:10.2514/6.1984-2074.

[28] Nguyen, L., Ogburn, M., Gilbert, W., Kibler, K., Brown, P., and Deal, P., "Simulator Study of Stall/Post-Stall Characteristics of a Fighter Airplane With Relaxed Longitudinal Static Stability," Technical Paper 1538, NASA, 1979.

[29] Soderman, P., and Aiken, T., "Full scale wind tunnel tests of a small unpowered jet aircraft with a t-tail," Technical Note D-6573, NASA, 1971.

[30] Etkin, B., and Reid, L., *Dynamics of Flight : Stability and Control*, John Wiley & Sons, INC., 1995, Chap. 6, pp. 171–175.

[31] Montgomery, R., and Moul, M., "Analysis of deep-stall characteristics of T-Tailed Aircraft Configurations and Some Recovery Procedures," *Journal of Aircraft*, Vol. 3, No. 6, 1966, pp. 562–566. doi:10.2514/3.43777.

[32] Abramov, N., Goman, M., Khrabrov, A., Kolesnikov, E., Sidoruk, M., Soemarwoto, B., and Smaili, H., "Aerodynamic model of transport airplane in extended envelope for simulation of upset recovery," *28th International Congress of the Aeronautical Sciences*, 2012.

[33] Khrabrov, A., Sidoryuk, M., and Goman, M., "Aerodynamic model development and simulation of airliner spin for upset recovery," *Progress in Flight Physics*, Vol. 5, 2013, pp. 621–636.

[34] Stengel, R., *Flight Dynamics*, Princeton University Press, 2004, Chap. B, pp. 810–813. ISBN: 0-691-11407-2.

[35] Thomas, H., and Collingbourne, J., "Longitudinal motions of aircraft involving high angles of attack," Reports and Memoranda 3753, Aeronautical Research Council, 1974.

[36] Guckenheimer, J., and Holmes, P., *Nonlinear Oscillations Dynamical Systems and Bifurcations of Vector Fields*, Springer-Verlag, New-York, 2000, Applied Mathematical Sciences, Vol. 42, Chaps. 1, 4. doi:10.1007/978-1-4612-1140-2.

[37] Stevens, B. L., and Lewis, F. L., *Aircraft Control and Simulation*, Wiley-Interscience, 2003, Chap. 4, pp. 261–270. doi: 10.1002/9781119174882.

[38] Hetru, L., "Étude expérimentale et numérique de l'interaction aérodynamique entre deux profils: application au risque aéronautique du décrochage profond," Ph.D. thesis, Université d'Aix Marseille, 2015.

[39] Wang, D., "Algebraic analysis of stability and bifurcation for nonlinear flight dynamics," *Aeronautical Journal*, Vol. 115, No. 1168, 2011, pp. 345–349. doi:10.1017/S0001924000005868.